Applied Catalysis B: Environmental 142–143 (2013) 579–589

Contents lists available at SciVerse ScienceDirect

Applied Catalysis B: Environmental

journal homepage: www.elsevier.com/locate/apcatb

Three-dimensional Z-scheme AgCl/Ag/γ-TaON heterostructural hollow spheres for enhanced visible-light photocatalytic performance

Jungang Hou, Chao Yang, Zheng Wang, Qinghuan Ji, Yitong Li, Guochao Huang, Shuqiang Jiao*, Hongmin Zhu

State Key Laboratory of Advanced Metallurgy, School of Metallurgical and Ecological Engineering, University of Science and Technology Beijing, Beijing 100083, China

ARTICLE INFO

Article history:
Received 8 April 2013
Received in revised form 30 May 2013
Accepted 31 May 2013
Available online 10 June 2013

Keywords:
Ag–AgCl nanocrystals
TaON hollow spheres
Photocatalyst
Degradation

ABSTRACT

Three-dimensional plasmonic Ag–AgCl/γ-TaON composites have been successfully synthesized by anchoring Ag–AgCl nanocrystals on the surfaces of monoclinic γ-TaON hollow urchin-like spheres via the deposition–precipitation method and photo-reduction process. The as-prepared samples were characterized by X-ray diffraction, scanning electron microscope, transmission electron microscope, Brunauer–Emmett–Teller analysis, X-ray photoelectron spectra and UV–vis diffuse reflectance spectrum. The interleaved nanoneedles assembled in the hierarchical floriated γ-TaON hollow spheres contributed to the stable deposition of Ag/AgCl nanocrystals and the formation of effective nanojunctions. The effects of the amount of Ag–AgCl nanocrystals and the photo-reduction time upon the photocatalytic properties for the Ag–AgCl/γ-TaON composites were systematically investigated. Inspiringly, the hierarchical AgCl/Ag/γ-TaON hollow composite photocatalyst in the Z-scheme system has the superior photocatalytic performance than γ-TaON hollow spheres and conventional β-TaON nanocrystals over the degradation of rhodamine B and acid orange 7 dyes and the reduction of aqueous Cr(VI), which is attributed to the effective charge transfer from plasmon-excited Ag nanocrystal to TaON, leading to the low recombination rates of the photoinduced electron–hole pairs. X-ray photoelectron spectroscopy analyses indicated that both AgCl and Ag^0 components coexist in the system, and the as-prepared composite is relatively stable. This work could provide new insights into the fabrication of hierarchically plasmonic photocatalysts with high performance and facilitate their practical application in environmental issues

1. Introduction

Solar fuel generation based on inexpensive, earth-abundant materials constitutes one potentially viable option to satisfy the demand for a terawatt scale renewable source of energy that can be stored and used on demand [1]. Environmental problems associated with harmful organic pollutants in water are the driving forces for sustained fundamental and applied research in the area of environmental remediation on the basis of highly efficient semiconductor photocatalysts using solar energy [2–4]. In recent decades, a large number of metal oxides as photocatalysts have been explored for the purpose of efficient degradation of harmful organic substances and hydrogen production through splitting water [5–9]. It is now generally recognized that nanoscale control of metal oxide architectures leads to the development of new materials and systems with unique physical and chemical properties [10–12]. To date, TiO_2, as a semiconductor photocatalyst with large band gap (about 3.2 eV), has been intensively investigated under UV irradiation (λ < 388 nm). However, the poor spectral response of the material as well as its relatively low efficiency of light utilization, due to its wide band gap (3.0–3.2 eV), limits its efficient use for solar energy harvesting [9,11]. More efficient visible light harvesting would render this material quite attractive for solar energy conversion. Among the potential candidates for water splitting, (oxy)nitride materials with a narrow band gap and the more negative potential of the nitrogen 2p orbital, have drawn considerable interest in photocatalysis due to their appropriate potentials [13]. For examples, $TiO_{2-x}N_x$ [14], Ta_3N_5 [15], TaON [16–19], $LaTiO_2N$ [20], and GaN:ZnO solid solution [5], have been extensively developed to induce the photocatalytic reaction under visible light irradiation. To the best of our knowledge, it is therefore highly desirable to develop a new modification and/or preparation method that can enhance the photocatalytic performance of (oxy)nitride nanostructures.

Recently, it is well demonstrated that three-dimensional (3D) hierarchically nanostructured materials that offers a large internal surface area with special morphology to effectively capture

* Corresponding author. Tel.: +86 10 62334775; fax: +86 10 62334204.
E-mail address: sjiao@ustb.edu.cn (S. Jiao).

0926-3373/$ – see front matter © 2013 Elsevier B.V. All rights reserved.
http://dx.doi.org/10.1016/j.apcatb.2013.05.078

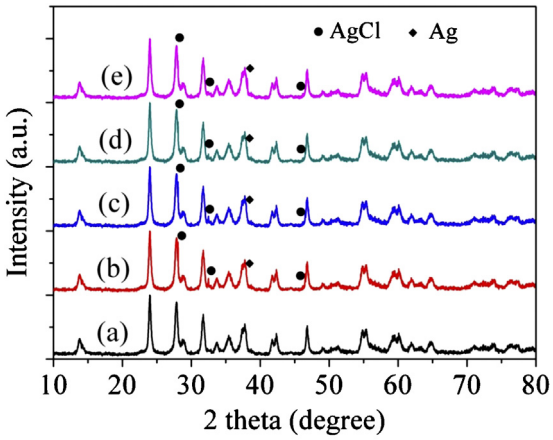

Fig. 1. XRD patterns of Ag–AgCl/γ-TaON composites for different photo-reduction times: (a) γ-TaON; (b) Ag–AgCl/γ-TaON–20; (c) Ag–AgCl/γ-TaON–30; (d) Ag–AgCl/γ-TaON–50; and (e) Ag–AgCl/γ-TaON–70.

incident illumination in combination with minimal charge transfer distance providing facile separation of photogenerated charge, exhibit enhanced properties compared to their bulk counterparts. As a result, continuous efforts are being made on the preparation of complex 3D oxide nanostructures [21–26]. Among them, 3D hollow structures with permeable shells and high surface area have emerged as an attractive material platform for water treatment.

To improve the photocatalytic performance, the use of heterojunction structures is an important strategy because it allows for the combination of properties from each element [27–29]. The heterojunction built not only can expand the spectral range of light-absorption, but also may promote photoexcited electron–hole separation which can minimize electron–hole recombination, thus significantly enhancing energy efficiency [30,31]. Furthermore, the surface plasmon resonance of metal nanoparticles has been introduced to photocatalysts due to the enhanced absorption in the visible light region [32–34]. For examples, Ag/AgCl/titanate honeycomb [35], Ag/AgCl@WO_3 [36], Ag/AgCl/ZnO [37], Ag/AgBr/TiO_2 [38], Ag/AgCl/BiOCl [39], Ag/AgX/GO (X = Cl, Br) [40], AgX/Ag_3PO_4 (X = Cl, Br, I) [41], have been applied for photocatalytic application. In addition, Dai et al. precipitated Ag/AgCl on P25 to synthesize Ag/AgCl/TiO_2 photocatalysts for photo-reduction of Cr(VI) and organic dyes [42]. Hou et al. reported Ag/AgCl/$Bi_{20}TiO_{32}$ photocatalysts were applied for photodegrdation of rhodamine B and acid orange 7 under visible-light irradiation [34]. Thus, there appears to be great untapped potential for exploring the possibility of using Ag–AgCl to improve photocatalytic activity with Ag–AgCl/TaON composites.

On the basis of the above survey, it seems logical that the best way to fabricate highly efficient photocatalysts may be to combine both approaches simultaneously, that is, coupling and nitriding (to get oxynitrides). In this work, the influences of synthesis parameters on the Ag–AgCl/TaON products, the synthesis mechanism, the critical roles of treatment conditions and catalyst compositions in determining catalytic performance, as well as the contribution of the work to the fields of visible-light photocatalytic activities were elaborated in detail. The effects of the amount of Ag–AgCl nanocrystals and the photo-reduction time upon the photocatalytic properties for the Ag–AgCl/TaON composites were systematically investigated. Compared with conventional TaON nanoparticles, the hierarchical γ-TaON with the hollow structure is advantageous for use as a supporting material for the stable deposition of Ag/AgCl nanocrystals and the formation of effective nanojunctions owing to the existence of the interleaving nanoneedles assembled in the hierarchical architecture. The significant improvement of photocatalytic performance of 3D monoclinic γ-TaON hollow urchin-like spheres coupled with Ag–AgCl nanocrystals in the degradation of rhodamine B (RhB) and acid orange 7 (AO7) and the reduction of harmful Cr(VI) solution under visible-light irradiation has been rarely reported. In addition, the photocatalytic mechanism of the Ag–AgCl/γ-TaON hollow composites was proposed. Hence, this work may be of interest to both materials scientists and those working in the area of catalyst design.

2. Experimental

2.1. Synthesis of γ-TaON hollow spheres

All chemicals were analytical grade and used without further purification. In a typical procedure, 1 g tantalum powder (black-color) was added to 20 mL of 1.33 mol L^{-1} hydrofluoric acid aqueous solution with 4.0 mL of 30 wt% hydrogen peroxide solution, heated at 240 °C in a Teflon-lined cylindrical autoclave. After cooling naturally, the tantalum oxide were separated, washed with ethanol for three times and then dried in oven at 60 °C for 12 h. In addition, γ-TaON samples were prepared by nitridation heat treatment of Ta_2O_5 powders via the controllable thermal time in our

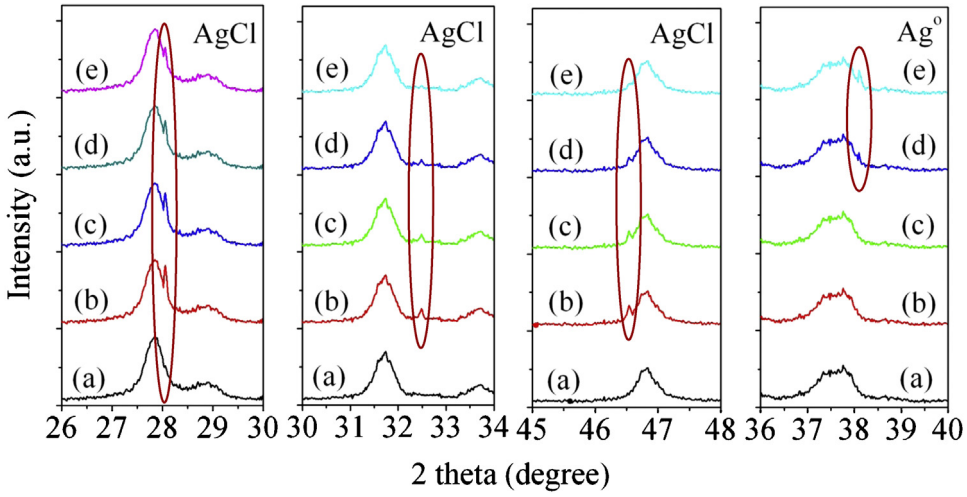

Fig. 2. Evolution of XRD patterns associated with a certain theta degree of Ag–AgCl/γ-TaON composites for different photo-reduction times: (a) γ-TaON; (b) Ag–AgCl/γ-TaON–20; (c) Ag–AgCl/γ-TaON–30; (d) Ag–AgCl/γ-TaON–50; and (e) Ag–AgCl/γ-TaON–70.

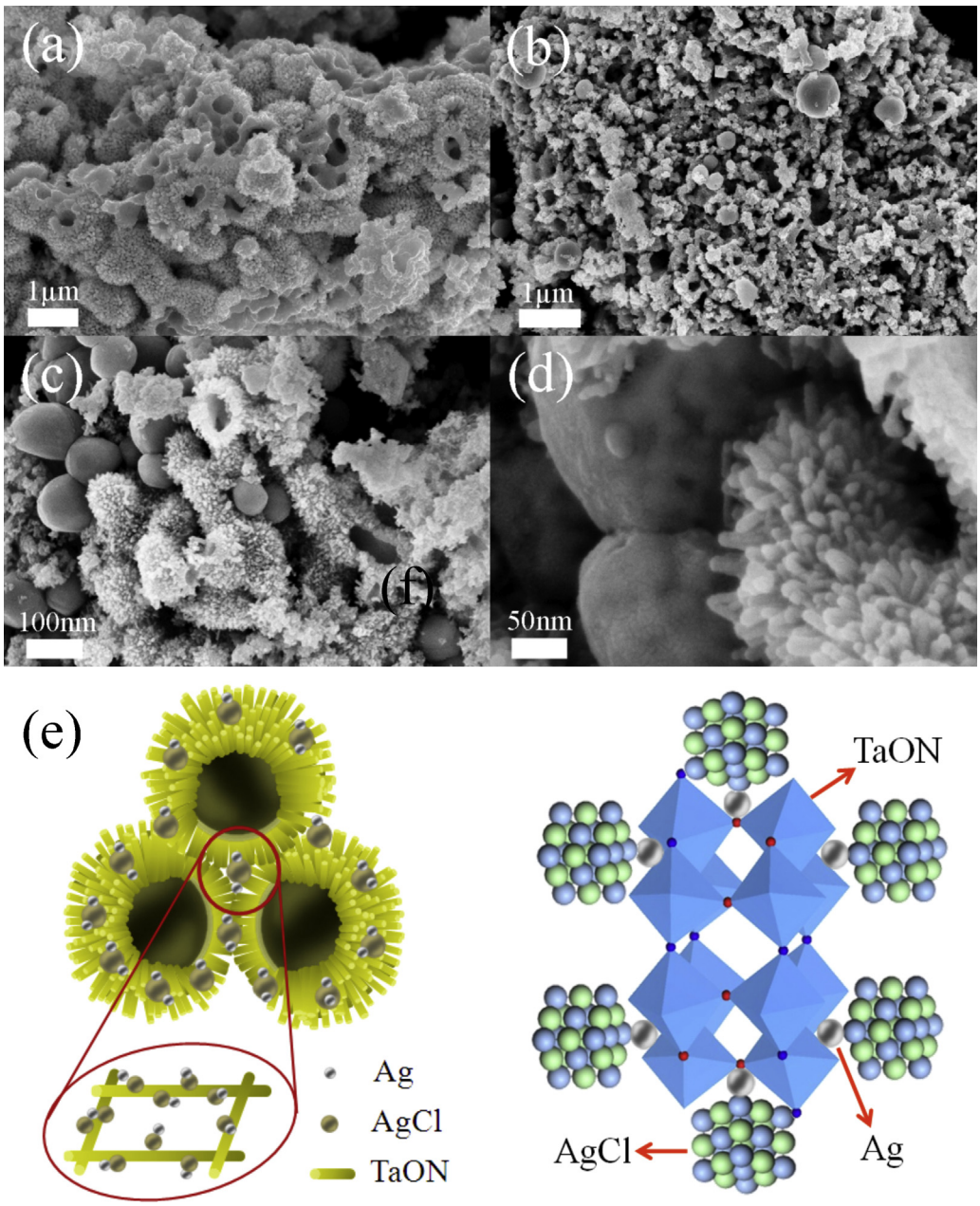

Fig. 3. SEM images of various samples. (a) γ-TaON hollow spheres, (b), (c), and (d) as-prepared hierarchical Ag–20 wt% AgCl/γ-TaON–50 photocatalysts, (e) and (f) schematic structures of Ag–AgCl/γ-TaON composites.

previous work [43]. Conventional β-TaON samples were synthesized according to the previous work [16].

2.2. Synthesis of hierarchical Ag–AgCl/γ-TaON composites

In a typical synthesis of Ag–AgCl/γ-TaON composites, 0.2 g of TaON hollow spheres and 0.3 g of hexadecyltrimethylammonium chloride (CTAC) were added to 100 mL of deionized water and the suspension was stirred for 60 min. Then 2.0 mL of 0.1 M $AgNO_3$ was quickly added to the above mixture. During this process, the excessive surfactant CTAC not only adsorbed onto the surface of γ-TaON hollow spheres to limit the number of nucleation sites for AgCl to grow, resulting in homogenously dispersed AgCl, but also induced Cl^- to precipitate Ag^+ in the suspension. The resulting suspension was stirred for 1.0 h and then placed under irradiation of 300 W Xe lamp for the indicated lengths of time. The suspension was9 filtered, washed with deionized water, and dried at 80 °C for 12 h. Depending on the duration of irradiation, the as-prepared catalysts were denoted as Ag–*n*AgCl/γ-TaON–*m* composites, where "*n*" represented 5, 10, 20 and 30 wt% of the amount of AgCl nanocrystals and "*m*" represented 20, 30, 50 and 70 min of photo-reduction time.

2.3. Characterization

The obtained products were characterized by powder X-ray diffraction (XRD, MAC Science Co. Ltd Japan) using Cu K_α ($\lambda = 0.1546$ nm) and XRD patterns were obtained at 10–90° by step scanning with a step size of 0.02°. The morphology and size of the resultant products were observed using a field emission scanning electron microscopy (FESEM, JEOL, JSM-6701F) with energy-dispersive spectra and transmission electron microscopy (TEM, JEM-2010) at an acceleration voltage of 200 kV. The optical

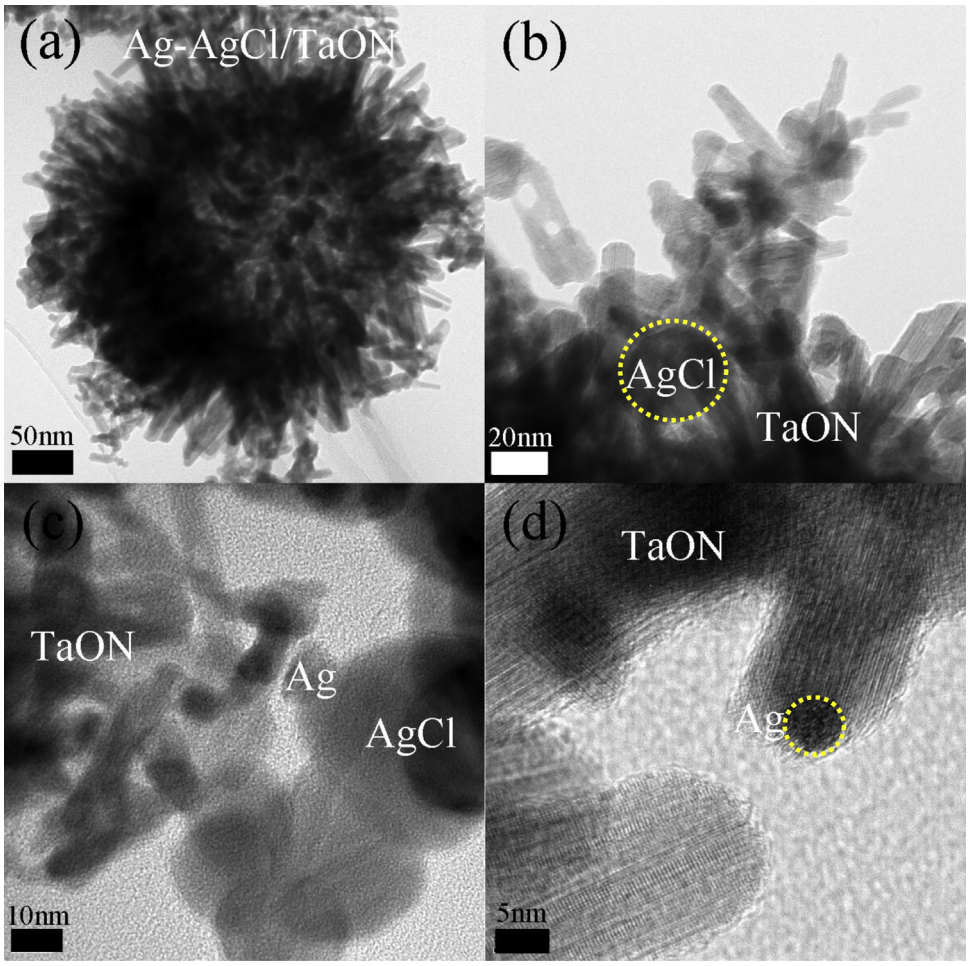

Fig. 4. TEM and HRTEM images of Ag–AgCl/γ-TaON composites with different magnigication.

properties of the samples were analyzed by UV–vis diffuse reflectance spectroscopy (UV–vis DRS) using a UV-vis spectrophotometer (UV-2550, Shimadzu) in the range 200–900 nm. The as-prepared sample was degassed at 200 °C prior to nitrogen adsorption measurements. The BET surface area was determined by a multipoint BET method using the adsorption data in the relative pressure (P/P_0) range of 0.05–0.3. A desorption isotherm was used to determine the pore size distribution via the Barret–Joyner–Halender (BJH) method. The chemical states of the sample were determined by X-ray photoelectron spectroscopy (XPS) in a VG Multilab 2009 system (UK) with a monochromatic Al K_α source and charge neutralizer.

2.4. Photocatalytic test

Photocatalysis reactions were performed in an air-free, closed gas circulation system with a quartz reaction cell at room temperature. Photocatalytic activity was evaluated by the degradation of rhodamine B (RhB) and acid orange 7 (AO7) in aqueous solution under visible-light irradiation using a 300 W Xe lamp with a cutoff filter ($\lambda > 420$ nm). A cylindrical Pyrex flask (200 mL) was placed in a sealed black box of which the top was open and the cutoff filter was set on the window face of the reaction vessel to ensure the desired irradiation condition. In each experiments, the samples as catalysts were added into rhodamine B (RhB), acid orange 7 (AO7) solution (1×10^{-4} M, 100 mL) and $K_2Cr_2O_7$ aqueous solution (1×10^{-4} M) in the presence of salicylic acid (5×10^{-5} M), respectively. For the 0.1 g Ag–AgCl/TaON composites as the catalysts were chosen for the evaluation of photocatalytic activity. Before illumination, the suspension between photocatalyst powders and rhodamine B (RhB) and acid orange 7 (AO7) at given time intervals (3 mL aliquots) were sampled and centrifuged to remove photocatalyst powders. And the Cr(VI) content in the supernatant solution was determined colorimetrically at 540 nm using the diphenylcarbazide method. The filtrates were analyzed by recording the variations of the absorption-band maximum (655 nm) in the UV–vis spectrum of dyes solution using a UV-vis spectrophotometer (Shimadzu 2550, Japan).

3. Results and discussion

3.1. Characterization of Ag–AgCl/γ-TaON composites

There has been an explosion of interest in Ag–AgCl nanocrystals based composite photocatalysts with appropriate energy band and appropriate band edge positions due to its potential applications in the physical, chemical, biological, photoelectric, and catalytic fields [32–42]. Figs. 1 and 2 show the XRD patterns of the as-prepared Ag/AgCl nanocrystals decorated the TaON catalysts. All the diffraction lines can be indexed as the monoclinic γ-TaON phase, cubic phase Ag and cubic phase AgCl, respectively, which are marked clearly in the XRD patterns. Especially, after photo-reducing AgCl under visible light irradiation for 0–30 min, three major diffraction peaks at 28.06°, 32.48° and 46.54° in the 2θ range of 10–80° (as shown in Fig. 2), which can be indexed to the (1 1 1), (2 0 0) and (2 2 0) reflections of a cubic silver chloride phase (space

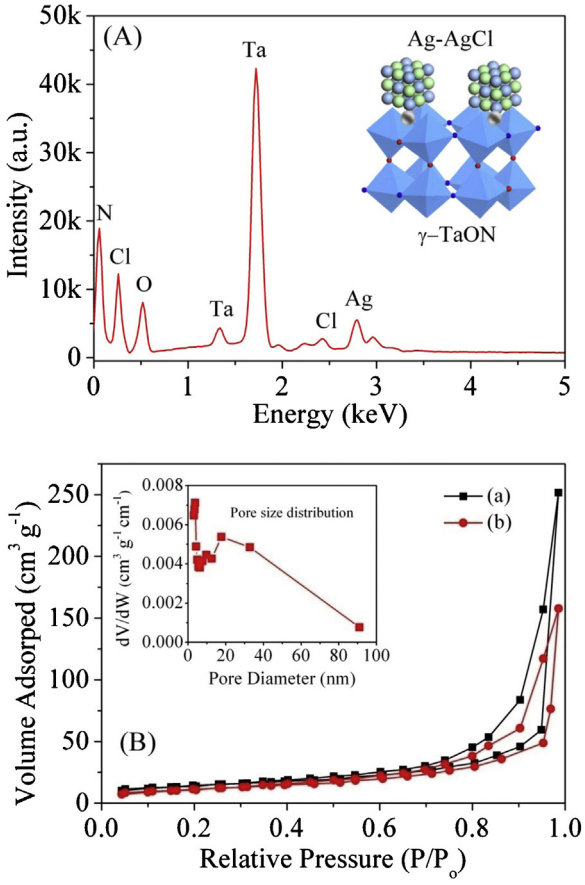

Fig. 5. (A) EDS image of the as-prepared hierarchical Ag–AgCl/γ-TaON photocatalysts; (B) full nitrogen sorption isotherms of as-prepared γ-TaON (a) and Ag–AgCl/γ-TaON composites (b). The inset is the corresponding pore-size distribution of the Ag–AgCl/γ-TaON composites.

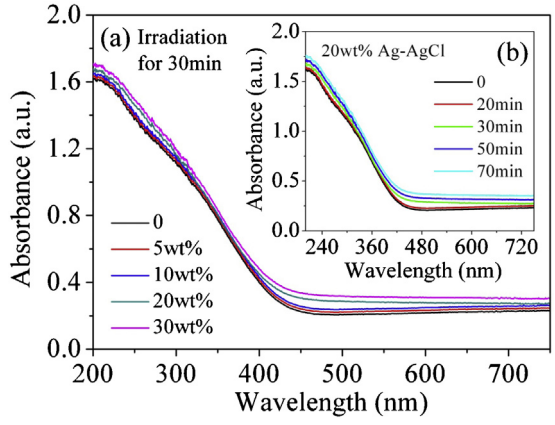

Fig. 6. The UV–vis spectra of (A) Ag–*n*AgCl/γ-TaON–50 using with different amount of Ag–AgCl nanocrystals: (a) 0, (b) 5 wt%, (c) 10 wt%, (d) 20 wt% and (e) 30 wt%; and (B) Ag–20 wt% AgCl/γ-TaON–*m* under various photo-reduction time: (a) 0, (b) 10 min, (c) 30 min, (d) 50 min and (e) 70 min.

group: Fm3m [225]) according to the JCPDS card (No. 31-1238). Currently, as the irradiation time increased, the intensity of peaks ascribed to AgCl decreased, indicating that some AgCl was photo-reduced, and the corresponding Ag nanoparticles were generated on the surface of Ag–AgCl/γ-TaON composites. However, there is no obvious reflections belonging to metal Ag species during this photo-reducing process for 0–30 min. Though the photo-reduction for 50–70 min, the Ag–AgCl/γ-TaON composites present a recognizable reflection at $2\theta = 38.1^\circ$ (as shown in Fig. 2) belonging to the metal Ag species in their XRD patterns. It is considered that the amount of the Ag species photo-induced is too small to detect by the XRD method for the sample, which is in agreement with the recent reports [34]. The result proved that the production of Ag^0 can be attributed to the pyrolysis of AgCl. Thus, it was clear that this method led to the successful formation of the Ag–AgCl/γ-TaON composite and the photo-reduction time plays a pivot role on the formation of the Ag–AgCl/γ-TaON composite.

The uniform hollow urchin-like hierarchical nanostructures consist of well-organized independent nanoneedles with the length of 100–200 nm (Fig. 3a). As shown in Fig. 3b and c, the as-prepared products are composed of the Ag–AgCl nanocrystals decorated on the surface of urchin-like γ-TaON structures. The magnified image shown in Fig. 3d presents that the urchin-like γ-TaON based composites are generated with very thin and long rod-like subunits pointing radially outward, coupling the dispersed Ag–AgCl nanocrystals. Previously, it's well known that the materials with hierarchical structures showed enhanced performance in energy conversion [44]. Besides, a decrease in the contact area and an increase in the distance among the particles will reduce the attractive force between colloidal particles, thereby avoiding the nanoparticle aggregation issues in the aqueous solution in theory [45]. So, we devise a typical process to prepare the uniformly distributed three-dimensional Ag–AgCl/γ-TaON heterostructural hollow spheres. In Fig. 3e and f, the schematic structures show that the intrinsic hydrothermal formation of γ-TaON structure is beneficial to the in situ growth of Ag–AgCl nanocrystals. Finally, the components of Ag–AgCl/γ-TaON composites include various abundant elements (silver, tantalum, nitrogen and oxygen) and therefore they are low-cost and amenable to large-scale implementations.

Typical TEM and HRTEM observations with different magnification of the as-prepared hierarchical three-dimensional Ag–AgCl/γ-TaON heterostructural hollow spheres are shown in Fig. 4, indicating that the Ag/AgCl nanocrystals are uniformly and firmly anchored on the surfaces of the γ-TaON hollow spheres. HRTEM images of Ag–AgCl/γ-TaON composites (Fig. 4) show the distinct crystallographic planes of Ag, AgCl and γ-TaON, respectively. Furthermore, the growth direction of the one dimensional interleaved nanoneedles assembled in the hierarchical floriated Ag–AgCl/γ-TaON hollow spheres nanojunctions can be indexed as the {0 0 1} zone axis of monoclinic γ-TaON [43].

The elemental composition and the content of elements of the Ag–AgCl/γ-TaON composite were examined by energy dispersive spectrometer. According to the corresponding energy dispersive spectra, Fig. 5A presents that the pristine TaON hollow spheres are composed of Ta, N and O as the component elements and the as-prepared Ag–AgCl nanocrystals consist of Ag, O, and Cl as the major elements. According to the EDS result, the surface atomic ratio of silver to chlorine was 1.4 times higher than the stoichiometric ratio in AgCl (1: 1), indicating the existence of excessive Ag nanocrystals on the surface. This hierarchical nanostructure is especially favorable for the enhancement of photocatalytic performance. Full nitrogen sorption isotherms of the Ag–AgCl/γ-TaON heterostructural hollow spheres were measured to gain the information about the specific surface area, as shown in Fig. 5B. After the BET measurement, it is found that there was no obvious difference before and after the deposition of Ag/AgCl on γ-TaON structures. The N_2 adsorption–desorption isotherms curves of photocatalysts are type IV isotherms. The pore-size distribution was also very similar for γ-TaON and Ag–AgCl/γ-TaON materials. N_2 adsorption and desorption results indicated that the introduction of Ag/AgCl had little effect on the structural properties of the γ-TaON support. The corresponding Barrett Joyner Halenda (BJH) analyses (the inset in Fig. 5B) exhibit that most of the pores fall into the size range from

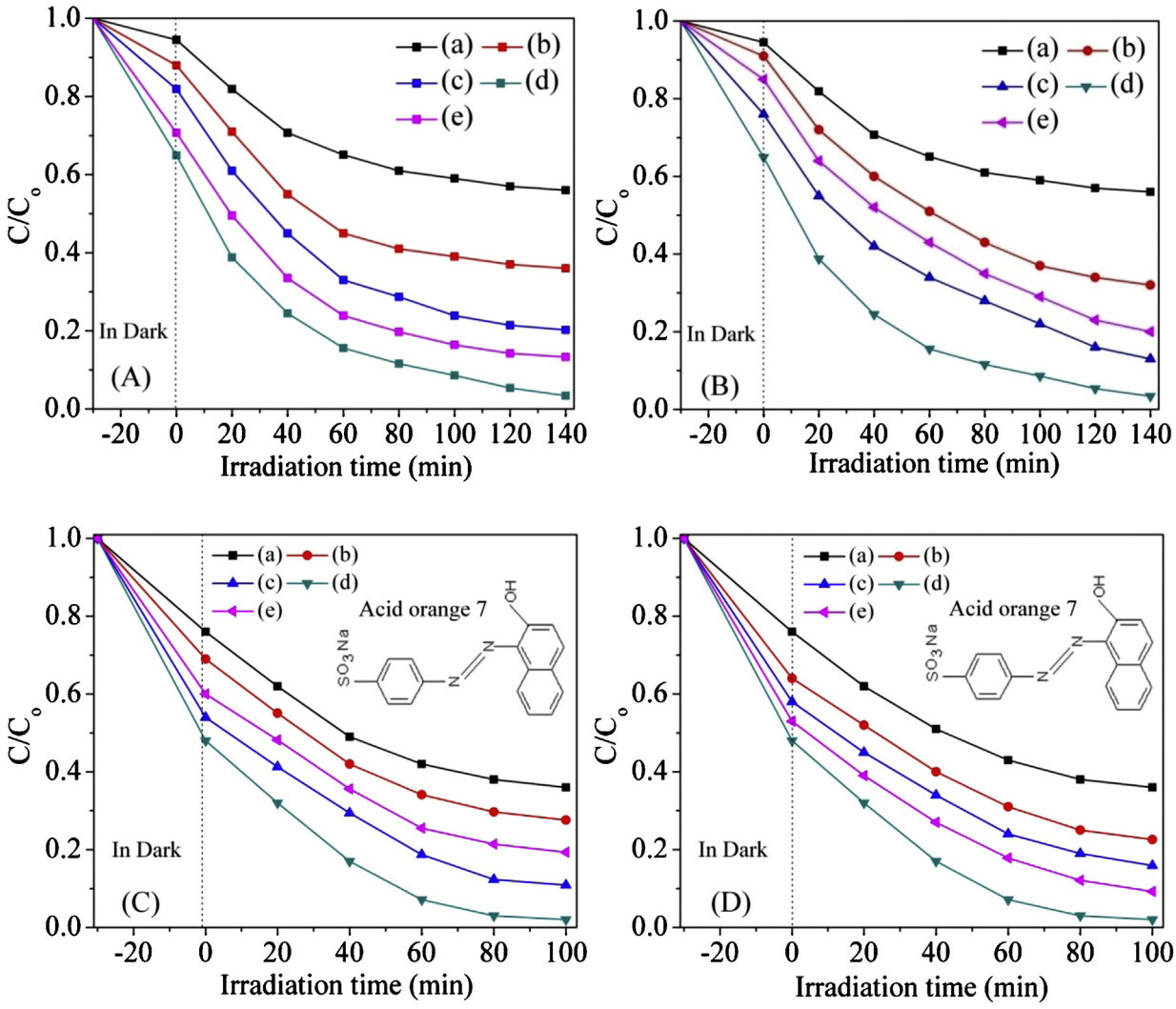

Fig. 7. Visible-light-driven photocatalytic degradation of RhB (A) and (B) and acid orange 7 (C) and (D) solution with various samples. (A) and (C) Ag–*n*AgCl/γ-TaON–50 using with different amount of Ag–AgCl nanocrystals: (a) 0 wt%, (b) 5 wt%, (c) 10 wt%, (d) 20 wt% and (e) 30 wt%; (B) and (D) Ag–20 wt% AgCl/γ-TaON–*m* under various photo-reduction time: (a) 0 min, (b) 10 min, (d) 30 min, (d) 50 min and (e) 70 min.

5 to 100 nm. These pores presumably arise from the spaces among the Ag–AgCl/γ-TaON composites. The high surface area and porous structure of the Ag–AgCl/γ-TaON composites provide the possibility for the efficient diffusion and transportation of the degradable organic molecules and hydroxyl radicals in photochemical reaction, which will lead to the enhanced photocatalytic performance of the Ag–AgCl/γ-TaON composites.

3.2. Light absorption and photocatalytic activities of Ag–AgCl/γ-TaON composites

The optical absorption of the Ag–AgCl/γ-TaON composites was measured by UV–vis diffuse reflection spectroscopy, as shown in Fig. 6. The Ag–AgCl/γ-TaON composites presented the wavelength range up to 500 nm for the visible light absorption. The band gap energies of the as-prepared γ-TaON hollow spheres and Ag–AgCl/γ-TaON composites are determined from a plot of $(ahv)^2$ vs energy (hv) and are found to be below 2.76 eV. The series of Ag–AgCl/γ-TaON photocatalysts exhibited broad absorption in the region of visible light, which is attributed to the surface plasmon resonance effect of the Ag species formed in situ on the surfaces of the AgCl nanocrystals [32–42]. Thus, the hybridization of Ag–AgCl nanocrystals and the γ-TaON hollow spheres is effective for the visible-light response of the composites, which is considered that utilizing visible light for driving photocatalytic reactions is a key challenge and visible light absorption of a material is a prerequisite for visible light activity.

The photocatalytic performance of the as-prepared conventional β-TaON nanocrystals, γ-TaON hollow spheres and Ag–AgCl/γ-TaON hollow composites samples were evaluated by monitoring the decomposition of rhodamine B (RhB) and acid orange 7 (AO7) in an aqueous solution and the reduction of aqueous Cr(VI) under visible light irradiation, respectively. The time-dependent UV–vis absorption spectra of RhB and AO7 dyes and aqueous Cr(VI) during the visible-light irradiation are displayed in Figs. 7 and 10. It can be seen clearly that the maximum absorbance decreases greatly after visible-light irradiation within 180 min for the as-prepared metastable TaON hollow spheres and the hierarchical Ag–20 wt% AgCl/γ-TaON-50 photocatalysts. Figs. 8 and 11 show the photodegradation of RhB and AO7 dyes and the reduction of aqueous Cr(VI) as a function of irradiation time for the various Ag–AgCl/γ-TaON samples. The obtained results for the degradation and reduction performance present that after visible-light irradiation, the photocatalytic activities for the Ag–AgCl/γ-TaON samples increased with the increase of the photo-reduction time among 0–50 min and the amount

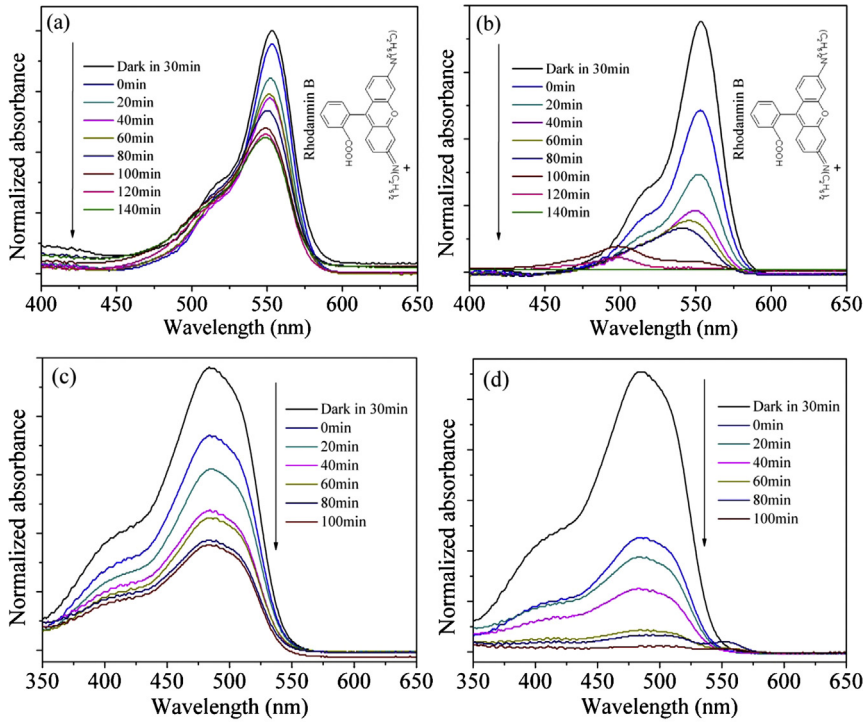

Fig. 8. UV–vis spectra changes in the degradation of RhB (A) and (B) and acid orange 7 (C) and (D) solution with various samples. (A) and (C) γ-TaON; (B) and (D) Ag–20 wt% AgCl/γ-TaON–50.

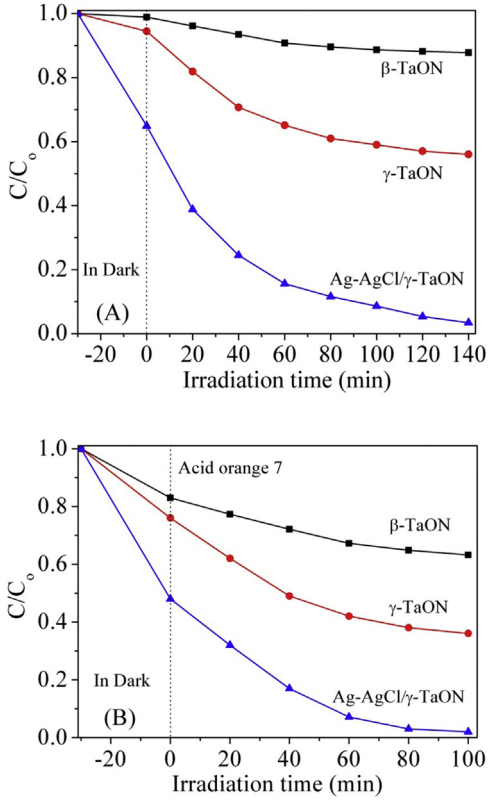

Fig. 9. Comparison for visible-light-driven photocatalytic degradation of RhB (A) and acid orange 7 (B) solution with β-TaON, γ-TaON and Ag–20 wt% AgCl/γ-TaON–50 samples.

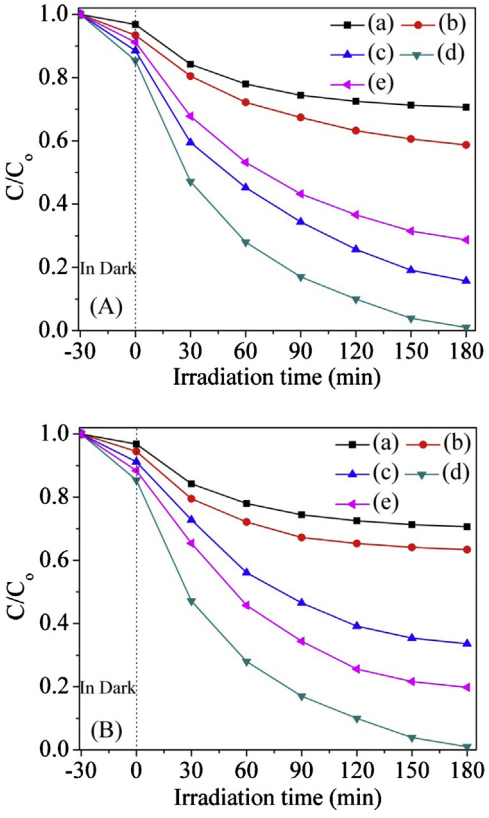

Fig. 10. Visible-light-driven photocatalytic reduction of aqueous Cr(VI) with various samples. (A) Ag–*n*AgCl/γ-TaON–50 using with different amount of Ag–AgCl nanocrystals: (a) 0 wt%, (b) 5 wt%, (c) 10 wt%, (d) 20 wt%, (e) 30 wt%; (B) Ag–20 wt% AgCl/γ-TaON–*m* under various photo-reduction time: (a) 0 min, (b) 10 min, (d) 30 min, (d) 50 min and (e) 70 min.

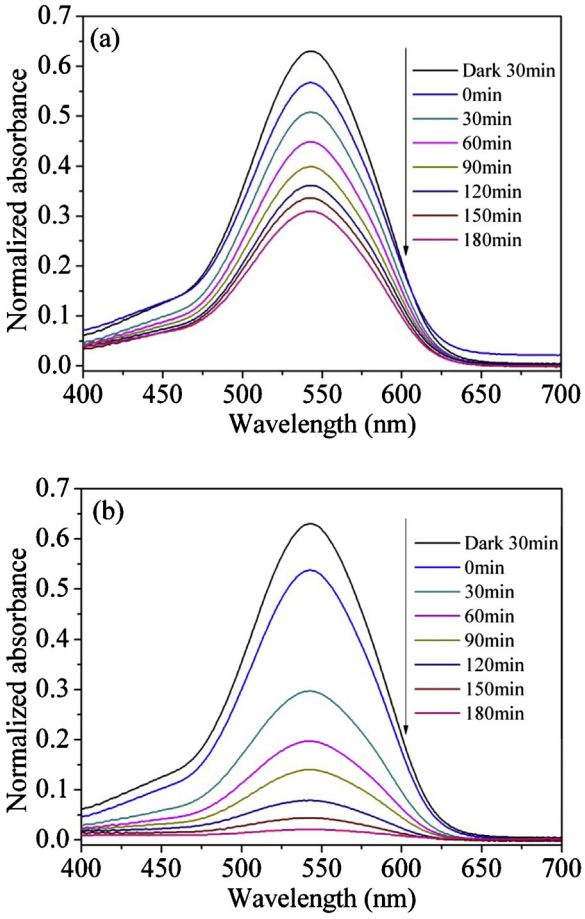

Fig. 11. UV–vis spectra changes in the reduction of aqueous Cr(VI) with (a) γ-TaON and (b) Ag–20 wt% AgCl/γ-TaON–50 samples.

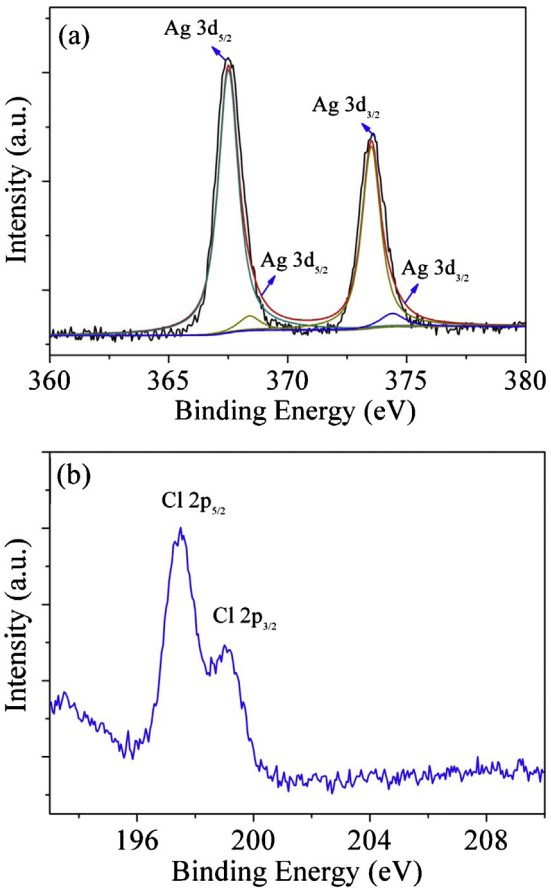

Fig. 13. XPS spectra of (a) Ag 3d and (b) Cl 2p for the Ag–20 wt% AgCl/γ-TaON–50 composite.

of Ag–AgCl nanocrystals between 0 and 20 wt%. However, the photocatalytic performance decreased with the increase of the photo-reduction time up to 70 min and the amount of Ag–AgCl nanocrystals up to 30 wt%. In addition, the visible-light-driven photocatalytic performance of β-TaON samples was also conducted in comparison (see Figs. 9 and 12). Among these samples, the Ag–20 wt% AgCl/γ-TaON-50 photocatalysts exhibited the most pronounced photocatalytic activity with the highest RhB and AO7 degradation efficiencies of about 96.6% (irradiation for 140 min) and 98.0% (irradiation for 100 min), respectively. Furthermore, the

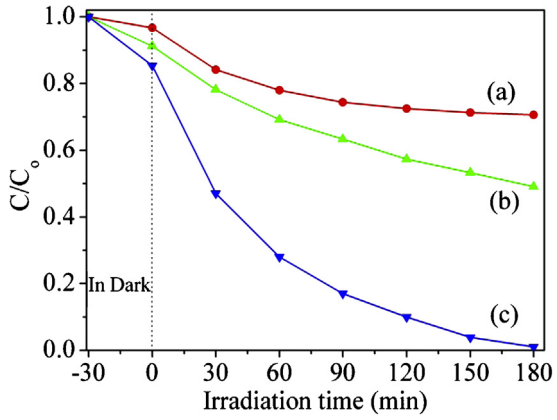

Fig. 12. Comparison for visible-light-driven photocatalytic reduction of aqueous Cr(VI) with β-TaON, γ-TaON and Ag–20 wt% AgCl/γ-TaON–50 samples.

superior photocatalytic reduction efficiency of aqueous Cr(VI) for the Ag–20 wt% AgCl/γ-TaON-50 photocatalysts was around 99.0% under the visible-light-driven irradiation for 180 min. As the duration of photo-reduction increased, the Ag nanoparticles content increased correspondingly, changing of the ratios of Ag^0/Ag^+. There should be an optimum ratio related to the best photocatalytic activity. For a fair comparison of all the Ag–AgCl/γ-TaON samples, the ratio of the Ag–20 wt% AgCl/γ-TaON-50 sample may best approach the optimum one. In order to examine the elemental composition, chemical status, and the content of elements of the Ag–20 wt% AgCl/γ-TaON-50 composite after photocatalytic reduction were examined by X-ray photoelectron spectroscopy. In the XPS spectra in Fig. 13(a) of the Ag 3d regions of the Ag–20 wt% AgCl/γ-TaON-50 sample, two peaks are observed at approximately 367.4 and 373.6 eV in each spectrum, which are ascribed to the Ag $3d_{5/2}$ and Ag $3d_{3/2}$ binding energies, respectively. These two peaks could be further deconvoluted into two peaks, at about 367.3/368.4 eV, and 373.6/374.6 eV, respectively. The peaks at 367.3 and 373.6 eV are attributed to Ag^+ of AgCl, and those at 368.4 and 374.6 eV are ascribed to the metal Ag^0. According to the results of the curve-fitting of Ag3d XPS spectrum, the atom ratio of metallic Ag to Ag^+ in the Ag–20 wt% AgCl/γ-TaON-50 composite is calculated to be 1:1.4. In the similar work, compared to the mole ratio of the $H_2WO_4{\cdot}H_2O$:Ag:AgCl composition, the relative ratio of Ag^0/Ag^+ in the $H_2WO_4{\cdot}H_2O$/Ag/AgCl composites prepared by a one-step ionic reaction between $Ag_8W_4O_{16}$/Ag nanorods and HCl aqueous solution, has been determined [48]. However, the ratio of Ag^0/Ag^+ increased as the duration of photo-reduction increased from 10 to 70 min, indicating that the excessive amount of silver might have been produced from the photo-reduction of AgCl on the

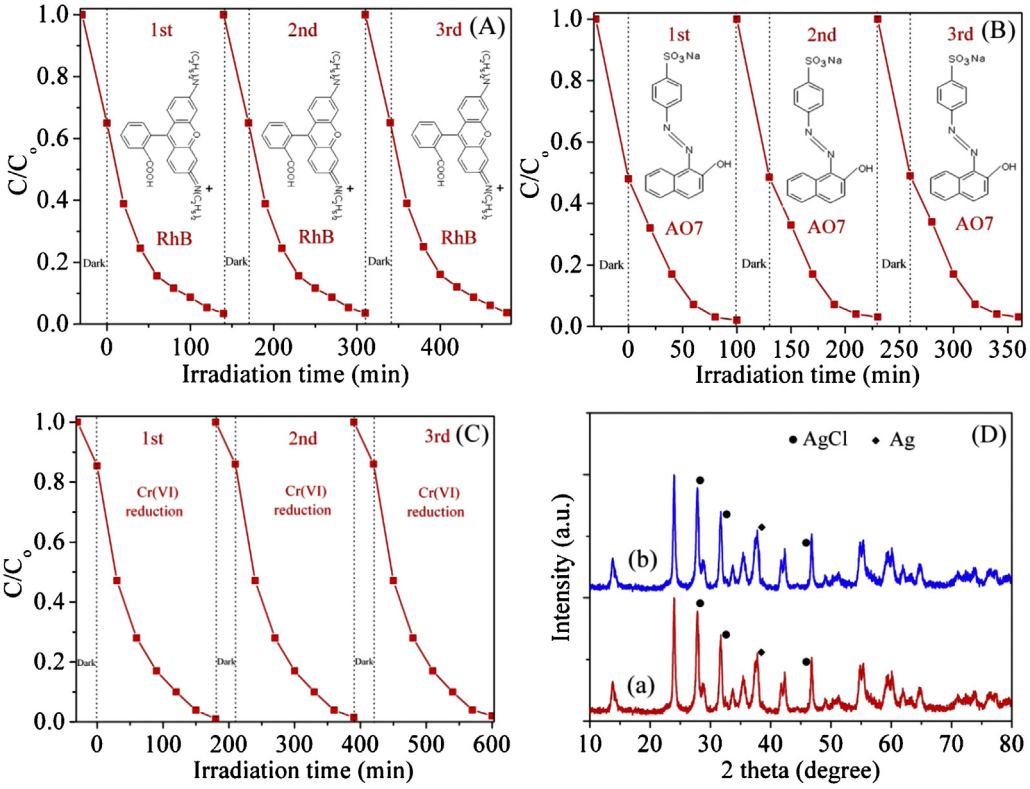

Fig. 14. Photocatalytic (A) RhB and (B) AO7 degradation and (C) harmful aqueous Cr(VI) reduction as well as (D) XRD patterns before (a) and after (b) photocatalysis of the hierarchical Ag–20 wt% AgCl/γ-TaON–50 photocatalysts under visible-light irradiation for three consecutive cycles.

surface. That is why the Ag–20 wt% AgCl/γ-TaON-70 sample with the more content of the Ag^0 on the surface of the sample, shows lower efficiency in photocatalytic activity. Thus, the enhancement of photocatalytic performance of the Ag–20 wt% AgCl/γ-TaON-50 composite is ascribed to the roles of Ag–AgCl nanocrystals.

The recycling properties of the hierarchical Ag–20 wt% AgCl/γ-TaON-50 photocatalyst for RhB, AO7 and harmful Cr(VI) solutions under visible-light irradiation (λ > 420 nm), as shown in Fig. 14, demonstrating a fairly stable photocatalytic performance for RhB and AO7 photodegradation and harmful Cr(VI) reduction. After a recycling application of three times, there is almost no obvious change for the photocatalytic performance of the Ag–AgCl/γ-TaON photocatalyst. The XRD patterns of the Ag–AgCl/γ-TaON sample after the recycling use indicates that the Ag content slightly increases but the major phases are still the AgCl nanocrystals and γ-TaON composites, as shown in Fig. 14.

To further understand the mechanism for the remarkably enhanced photocatalytic performance of the Ag–AgCl/γ-TaON photocatalysts from the following aspects. Firstly, the existence of Ag/AgCl nanocrystals on the surfaces of the γ-TaON hollow spheres forms an uniquely hierarchical nanostructure, which provides a high surface area and a large number of interfaces between the Ag/AgCl and γ-TaON species. The high surface areas and profuse interfaces are accessible to the outer environment, and provide numerous active sites for the photodegradation of dye molecules. Secondly, the metal Ag clusters formed in situ on the semiconductors AgCl and the γ-TaON nanocrystals remarkably enhance the absorption in the visible light region due to the surface plasmonic resonance effect, as shown in Fig. 15, which photogenerates transient holes that can oxidize the dye molecules [36,42]. Last but not least, the positively synergistic effects of the coupling of Ag/AgCl and the γ-TaON hollow spheres improve the effective separation of the photo-generated electron–hole pairs.

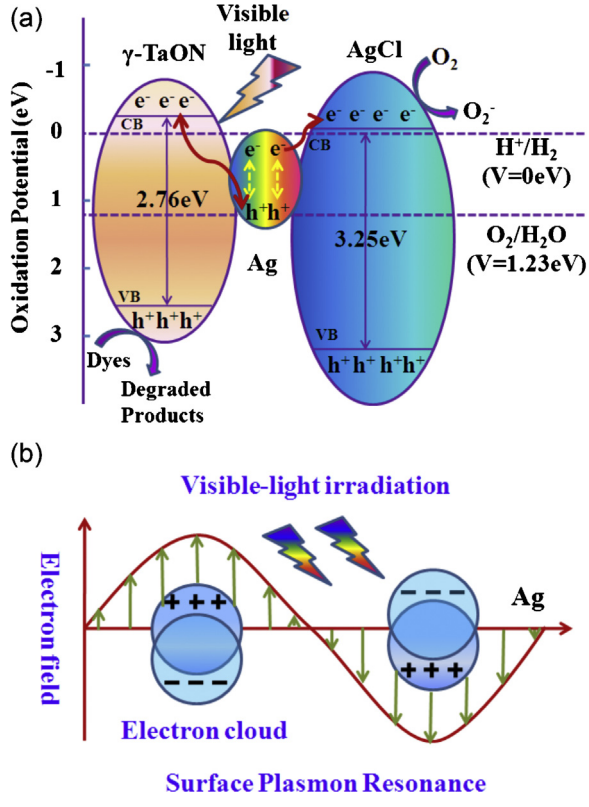

Fig. 15. (a) Schematic illustration of the charge separation and transfer in the AgCl/Ag/γ-TaON composites under visible-light irradiation; and (b) schematic for the surface plasmon resonance (SPR) effect of Ag nanocrystals.

The possible transfer routes of the photo-generated electrons and holes are also introduced to explain the enhanced photocatalytic activity using the conduction band minimum (CBM) and valence band maximum (VBM) potentials of Ag/AgCl and γ-TaON. Besides, the CB and VB energy levels of AgCl are calculated to be ca. −0.06 and +3.2 V (vs SHE) [44,45,36,46,47], respectively. According to the previous work from the flat-band potentials of γ-TaON and β-TaON are estimated to be −0.65 V and −0.6 V vs. SCE (−0.41 V and −0.36 V vs. NHE) [43]. So, the CB energy level of γ-TaON is more negative than the E_{cb} of β-TaON. On the basis of the above experimental results and band structure analysis of Ag/AgCl and γ-TaON, a plasmonic Z-scheme mechanism of AgCl/Ag/γ-TaON composite in a Z-scheme photocatalytic system is proposed and shown in Fig. 15. Under visible-light irradiation, the γ-TaON hollow spheres can absorb visible-light photons to produce photogenerated electrons and holes. Due to the surface plasmonic resonance effect and dipolar character of metallic Ag, metallic Ag can also absorb visible light, and the absorbed photon would be efficiently separated to an electron and a hole [44–48]. The plasmon-induced electrons of Ag nanoparticles are transported to the CB of AgCl. As a consequence, a relative high concentration of electrons on the surface of AgCl is formed, which can be trapped by O_2 and H_2O at the surface of photocatalysts to form $\bullet O^{2-}$, •OH radicals and other reactive oxygen species. These reactive oxygen species also help the degradation of dye molecules. While the holes remain on the Ag nanoparticles. Currently, the photogenerated electrons of γ-TaON hollow spheres transfer to the Ag nanoparticles to recombine with the plasmon-induced holes produced by plasmonic absorption of Ag nanoparticles, while the VB holes remain on γ-TaON hollow spheres to oxidize organic substances. So, such electron transfer from Ag to a semiconductor should be expected to facilitate the photoexcited electron to be separated from recombination with the hole. Besides, achieving the efficient Cr(VI) reduction for Ag–AgCl/γ-TaON photocatalysts, the photogenerated electron from γ-TaON hollow spheres and AgCl nanocrystals reduces Cr(VI) to Cr(III), and the concomitant oxidation of salicylic acid as the sacrificial electron donor contributes significantly to the photoactivity through the charges separation of electron and hole pairs. Therefore, the hierarchical AgCl/Ag/γ-TaON nanojunction photocatalysts in a Z-scheme system exhibit excellent photocatalytic performance.

4. Conclusion

The hierarchical photocatalysts of Ag–AgCl/γ-TaON hollow spheres composites have been successfully synthesized by anchoring Ag–AgCl nanocrystals on the surfaces of γ-TaON hollow spheres via the deposition–precipitation method and photo-reduction process. The amount of Ag–AgCl nanocrystals and the photo-reduction time for the Ag–AgCl/γ-TaON hollow spheres composites have appreciable effects on their photocatalytic performance. The 20 wt% Ag–AgCl nanocrystals with the photo-reduction time for 50 min, displayed the highest photocatalytic activity over the degradation of RhB and AO7 dyes and the reduction of harmful Cr(VI) solution. The enhanced photocatalytic performance in the Z-scheme system is attributed to the hierarchical structures with profuse interfacial active sites due to high surface areas and the effective charge transfer from plasmon-excited Ag nanocrystal to γ-TaON, leading to the low recombination rates of the photoinduced electron–hole pairs. The present work has paved a new way to achieve highly efficient photocatalysts with promising applications in environmental purification and energy conversion.

Acknowledgements

This work was supported by National Science Foundation of China (No. 51102015, 21071014 and 51004008), the Fundamental Research Funds for the Central Universities (No. FRF-AS-11-002A and FRF-TP-12-023A), China Postdoctoral Science Foundation (No. 20110490009), Research Fund for the Doctoral Program of Higher Education of China (No. 20110006120027), National High Technology Research and Development Program of China (863 Program, No. 2012AA062302), National Basic Research Program of China (973 Program, No. 2013CB632400) and the Program for New Century Excellent Talents in University (NCET-11-0577).

References

[1] N.S. Lewis, D.G. Nocera, Proceedings of the National Academy of Sciences of the United States of America 103 (2006) 15729–15735.
[2] Z.G. Yi, J.H. Ye, N. Kikugawa, T. Kako, S.X. Ouyang, H. Stuart-Williams, H. Yang, J.Y. Cao, W.J. Luo, Z.S. Li, Y. Liu, R.L. Withers, Nature Materials 9 (2010) 559–564.
[3] J.G. Hou, R. Cao, Z. Wang, S.Q. Jiao, H.M. Zhu, Journal of Hazardous Materials 217/218 (2012) 177–186.
[4] J.G. Hou, Z. Wang, S.Q. Jiao, H.M. Zhu, CrystEngComm 14 (2012) 5923–5928.
[5] K. Maeda, K. Teramura, D. Lu, T. Takata, N. Saito, Y. Inoue, K. Domen, Nature 440 (2006), 295–295.
[6] J.G. Hou, Y.F. Qu, D. Krsmanovic, C. Ducati, D. Eder, R.V. Kumar, Chemical Communications 26 (2009) 3937–3939.
[7] X.C. Wang, K. Maeda, A. Thomas, K. Takanabe, G. Xin, J.M. Carlsson, K. Domen, M. Antonietti, Nature Materials 8 (2009) 76–82.
[8] J.G. Hou, Y.F. Qu, D. Krsmanovic, C. Ducati, D. Eder, R.V. Kumar, Journal of Materials Chemistry 20 (2010) 2418–2423.
[9] X. Chen, S. Mao, Chemical Reviews 107 (2007) 2891–2959.
[10] J.G. Hou, R. Cao, S.Q. Jiao, H.M. Zhu, R.V. Kumar, Applied Catalysis B: Environmental 104 (2011) 399–406.
[11] A. Kudo, Y. Miseki, Chemical Society Reviews 38 (2009) 253–278.
[12] J.G. Hou, R. Cao, Z. Wang, S.Q. Jiao, H.M. Zhu, Journal of Materials Chemistry 11 (2011) 7296–7301.
[13] K. Maeda, K. Domen, The Journal of Physical Chemistry C 111 (2007) 7851–7861.
[14] R. Asahi, T. Morikawa, T. Ohwaki, K. Aoki, Y. Taga, Science 293 (2001) 269–271.
[15] G. Hitoki, A. Ishikawa, T. Takata, J.N. Kondo, M. Hara, K. Domen, Chemistry Letters 31 (2002) 736–737.
[16] J.G. Hou, R. Cao, Z. Wang, S.Q. Jiao, H.M. Zhu, Dalton Transactions 40 (2011) 4038–4041.
[17] G. Hitoki, T. Takata, J.N. Kondo, M. Hara, H. Kobayashi, K. Domen, Chemical Communications 16 (2002) 1698–1699.
[18] J.G. Hou, Z. Wang, W.B. Kan, S.Q. Jiao, H.M. Zhu, R.V. Kumar, Journal of Materials Chemistry 22 (2012) 7291–7299.
[19] M. Higashi, K. Domen, R. Abe, Journal of the American Chemical Society 134 (2012) 6968–6971.
[20] F.X. Zhang, A. Yamakata, K. Maeda, Y. Moriya, T. Takata, J. Kubota, K. Teshima, S. Oishi, K. Domen, Journal of the American Chemical Society 134 (2012) 8348–8351.
[21] J.G. Hou, C. Yang, Z. Wang, S.Q. Jiao, H.M. Zhu, Applied Catalysis B: Environmental 129 (2013) 333–341.
[22] D. Chen, J.H. Ye, Advanced Functional Materials 18 (2008) 1922–1928.
[23] C. Yan, D. Xue, Advanced Materials 20 (2008) 1055–1058.
[24] Z. Wang, J.G. Hou, C. Yang, S.Q. Jiao, K. Huang, H.M. Zhu, Physical Chemistry Chemical Physics 15 (2013) 3249–3255.
[25] A. Hameed, T. Montini, V. Gombac, P. Fornasiero, Journal of the American Chemical Society 130 (2008) 9658–9659.
[26] Z. Wang, J.G. Hou, S.Q. Jiao, K. Huang, H.M. Zhu, Journal of Materials Chemistry 22 (2012) 21972–21978.
[27] J.G. Hou, Z. Wang, S.Q. Jiao, H.M. Zhu, Journal of Hazardous Materials 192 (2011) 1772–1779.
[28] J. Zhang, J.G. Yu, Y.M. Zhang, Q. Li, J.R. Gong, Nano Letters 11 (2011) 4774–4779.
[29] J.Z. Su, L.J. Guo, N.Z. Bao, C.A. Grimes, Nano Letters 11 (2011) 1928–1933.
[30] S.Y. Reece, J.A. Hamel, K. Sung, T.D. Jarvi, A.J. Esswein, J.J.H. Pijpers, D.G. Nocera, Science 334 (2011) 645–648.
[31] A. Paracchino, V. Laporte, K. Sivula, M. Gratzel, E. Thimsen, Nature Materials 10 (2011) 456–461.
[32] D. Tsukamoto, Y. Shiraishi, Y. Sugano, S. Ichikawa, S. Tanaka, T. Hirai, Journal of the American Chemical Society 134 (2012) 6309–6315.
[33] W.A. Murray, W.L. Barnes, Advanced Materials 19 (2007) 3771–3782.
[34] J.G. Hou, Z. Wang, C. Yang, W.L. Zhou, S.Q. Jiao, H.M. Zhu, The Journal of Physical Chemistry C 117 (2013) 5132–5141.
[35] H.G. Yua, R. Liu, X.F. Wang, P. Wang, J.G. Yu, Applied Catalysis B: Environmental 111/112 (2012) 326–333.
[36] D.L. Chen, T. Li, Q.Q. Chen, J.B. Gao, B.B. Fan, J. Li, X.J. Li, R. Zhang, J. Sun, L. Gao, Nanoscale 4 (2012) 5431–5439.
[37] Y.G. Xu, H. Xu, H.M. Li, J.X. Xia, C.T. Liu, L. Liu, Journal of Alloys and Compounds 509 (2011) 3286–3292.
[38] G. Tian, Y. Chen, H.L. Bao, X. Meng, K. Pan, W. Zhou, C. Tian, J.Q. Wang, H.G. Fu, Journal of Materials Chemistry 22 (2012) 2081–2088.
[39] W. Xiong, Q. Zhao, X. Li, D. Zhang, Catalysis Communications 16 (2011) 229–233.
[40] M. Zhu, P. Chen, M. Liu, ACS Nano 5 (2011) 4529–4536.

[41] Y.P. Bi, S.X. Ouyang, J.Y. Cao, J.H. Ye, Physical Chemistry Chemical Physics 13 (2011) 10071–10075.
[42] J.F. Guo, B. Ma, A. Yin, K. Fan, W.L. Dai, Journal of Hazardous Materials 211/212 (2012) 77–82.
[43] Z. Wang, J.G. Hou, C. Yang, S.Q. Jiao, K. Huang, H.M. Zhu, Energy and Environmental Science (2013), http://dx.doi.org/10.1039/C3EE24370B (in press).
[44] S. Yin, Y. Zhang, J. Kong, C. Zou, C. Li, X. Lu, J. Ma, F.Y.C. Boey, X. Chen, ACS Nano 5 (2011) 3831–3838.
[45] J.Y. Luo, H.D. Jang, T. Sun, L. Xiao, Z. He, A.P. Katsoulidis, M.G. Kanatzidis, J.M. Gibson, J.X. Huang, ACS Nano 5 (2011) 8943–8949.
[46] S. Linic, P. Christopher, D.B. Ingram, Nature Materials 10 (2011) 911–921.
[47] R. Liu, P. Wang, X.F. Wang, H.G. Yu, J.G. Yu, The Journal of Physical Chemistry C 116 (2012) 17721–17728.
[48] X.F. Wang, S.F. Li, Y.Q. Ma, H.G. Yu, J.G. Yu, The Journal of Physical Chemistry C 115 (2011) 14648–14655.